*Journal of The Electrochemical Society*, **165** (10) A2019-A2025 (2018)
0013-4651/2018/165(10)/A2019/7/$37.00 © The Electrochemical Society


# Grand Canonical Monte Carlo Study of Li Intercalation into Graphite

**E. M. Gavilán-Arriazu,[1,2] O. A. Pinto,[2] B. A. López de Mishima,[2] E. P. M. Leiva,[1] and O. A. Oviedo [1,z]**

[1] *Instituto de Fisicoquímica de Córdoba (INFIQC-CONICET), Departamento de Química Teórica y Computacional de la Facultad de Ciencias Químicas, Universidad Nacional de Córdoba, Córdoba X5000HUA, Argentina*
[2] *Instituto de Bionanotecnología del NOA (INBIONATEC-CONICET), Universidad Nacional de Santiago de Estero, Santiago del Estero G4206XCP, Argentina*

A computational model is proposed to study lithium-graphite intercalation compounds in the framework of Monte Carlo simulations in the Gran Canonical Ensemble. The results suggest the existence of fractional stages between stages II and I, which are rarely found in most experimental electrochemical measurements. These fractional stages seem to be part of a more general intercalation mechanism suggested for other intercalation compounds. The thermodynamic information obtained from the simulations for these fractional states at room temperature is discussed in the context of experimental data. In addition, clear evidence was found for the existence of a new stage, supported by recent experimental measurements.
 [DOI: 10.1149/2.1211809jes]

Manuscript submitted April 5, 2018; revised manuscript received May 30, 2018. Published June 30, 2018.

At present, most of the world's energy demand is satisfied through thermal combustion, which has resulted in a depletion of fossil fuel reserves and an increase in environmental pollution. For this reason, there are great efforts to achieve the independence from oil as energy source, substituting fossil fuel by renewable energy sources, coupled with battery banks as storage devices. Of all rechargeable batteries on the market, those based on Li-ion have numerous advantages: i) the working voltage provides a high energy storage density, ii) low cost, iii) easy handling, iv) good chemical stability and v) excellent electrochemical performance.[1,2] Thus, great efforts are being made to improve the durability and cycle life of this type of batteries.[3–6] To carry out this purpose, it is necessary to understand the physicochemical mechanisms that operate at molecular scale. It is in this context that computer simulations play a crucial role.

In the Li-ion batteries industry, graphite as anode material is the most commercialized form, since it presents a theoretical capacity of 372 mAh/g.[7] In a graphite Li-ion battery, lithium migrates between the electrodes during the loading and unloading process. The intercalation process can be described as:

$$C_6 + x\ Li^+ + x\ e^- \rightarrow Li_xC_6 \qquad [1]$$

Where $x$ corresponds to the Li composition in the graphite matrix. It is widely recognized that Li intercalation in these materials result in different stages, generally known as Lithium Graphite Intercalation Compounds (LGIC). Most of these stages have been detected and studied by electrochemical and X-ray diffraction techniques,[8–10] which allow structure determination. Another property, important for the characterization of LGICs is the intercalation entropy, which can be studied from experimental[11] or theoretical approaches.[12] There is an overall agreement to identify the LGICs as: "stage *n/m*". This quotient represents the minimum periodic structure composed of $m$ Li layers which are repeated every $n$ graphite sheets. Hence, stages where $m = 1$ correspond to the so-called "entire" stages (1, 2, 3, 4, etc.), generally designed with roman numerals (I, II, III, IV, etc). On the other hand, stages with $m > 1$ are called "fractional stages".[13] For example, the fractional stage composed of three sheets filled with lithium between four graphite sheets is called "stage 4/3".

When the anode is completely discharged, the thermodynamically stable form of graphite is that with ABAB stacking sequence. However, when lithium is intercalated between the graphite sheets, reaching the stage I formation, the stacking sequence changes to AAAA.[14,15] The real situation is probably more complex, since it has been proposed the existence of several ABAA and AABB hybridized structures between the sequences previously described.[9] One hypothesis to explain the carbon planes sliding (ABAB → AAAA), suggests that the intercalated Li atoms perturb and shield the van der Waals forces between the carbon sheets, producing the change in the stacking sequence.[16] It has also been proposed that this perturbation is dependent on the Li concentration in each graphite layer, an assumption that has not been verified experimentally yet.

Very recent experimental results,[17] involving entropy hysteresis phenomenon, propose a transition mechanism between stages II and IV (and vice versa) where the stage III is not present. Instead, this new mechanism suggests the existence of a new stage, mixture of stages IV and II, called stage 4-2 (for lithiation) and stage 2–4 (for delithiation).

In the computational simulation field based on DFT, Pande,[18] Persson,[16] Sascha[19] and Robledo[20] have demonstrated the need to include van der Waals interactions to describe the system in a better way. Recently, Raju et al have implemented Grand Canonical Monte Carlo and Molecular Dynamics schemes applying reactive potentials - ReaxFF[21] -, allowing access to simulations at finite temperature. Alternatively, Perassi and Leiva[12] presented a model based on the interaction potential of Derosa,[22] applying the Monte Carlo technique in the Grand Canonical ensemble. This study compared the entropy and differential enthalpy of intercalation of stage II and stage I with experimental data. We have used a similar model in a recent work to study the phase transition of LGIC stage II.[23]

The present work is focused on the analysis of the complete intercalation process of lithium in graphite. To tackle this issue, we have modified the interaction potential previously reported by Perassi[12] using a Monte Carlo Grand Canonical scheme. Such an approach has been found recently very useful to understand the influence of point defects on the entropy profiles of lithium ion battery cathodes.[24] The present article is organized as follows: Section Model and computations presents details related to the system, potential energy and computational methods. Then, we present the main results of the simulations and a discussion is proposed. Finally, section Discussion presents the most relevant conclusions.

## Model and Computations

***The systems.—***The simulation cell was constructed with 24 graphite planes with the AAAA stacking sequence, where each plane contains 288 carbon atoms arranged in a honeycomb-like structure (hexagonal lattice). Therefore, the simulation cell contains a total of 6912 carbon atoms, generating a grid of sites available for Li intercalation. Periodic boundary conditions were employed in all three directions. The z-direction was chosen perpendicular to the surface, while the x-y plane was considered parallel to the graphite planes.

To construct the cell, the following steps were followed: a graphene sheet was built with the lattice parameter measured in bulk graphite

[z] E-mail: o.a.oviedo@unc.edu.ar

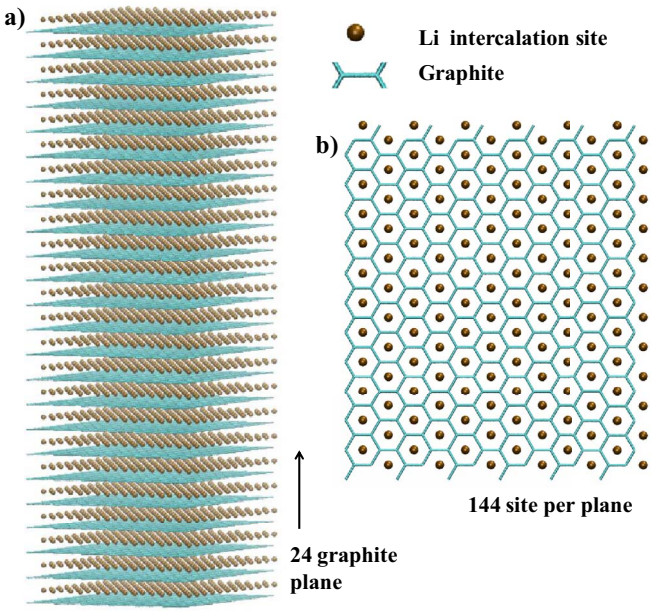


**Figure 1.** Scheme of the simulation cell employed to represent the graphite substrate plus Li-intercalation sites. It consists of a 24 layers graphene slab. a) Side view (x-z plane). b) Top view of the cell (x-y plane). Periodic boundary condition in x, y and z directions were applied. Gray and green spheres correspond to the carbon and Li atoms, respectively.

at 296 K (1.42Å).[25] This sheet was then replicated along the z coordinate using a displacement distance of 3.35 Å between the carbon sheets. Figure 1 shows two pictures of the simulation cell in different perspectives, a) x-z plane and b) x-y plane.

***Potential energy.—***The potential energy of a single intercalated Li particle was:

$$E = E^{L-J} + E^{I-I} + E^{A} \quad [2]$$

where,

$$E^{L-J} = \varepsilon\left[\left(\frac{r_m}{r}\right)^{12} - 2\left(\frac{r_m}{r}\right)^{6}\right] \quad [3a]$$

$$E^{I-I} = D_0 {r_b}^{\alpha}\left(\frac{1-e^{-\beta r}}{r^{\alpha}}\right) \quad [3b]$$

$$E^{A} = \gamma \quad [3c]$$

Equation 3a is used to emulate pairwise interactions between Li atoms in the same plane. For this purpose, a Lennard-Jones potential term was used, $E^{L-J}$, described in detail in the References 12 and 26. $\varepsilon$ is the depth of the potential well at a distance $r_m$, which corresponds to second neighbors, and $r$ is the distance between lithium pairs in the same plane. Since this term is repulsive to first neighbors, there is a strong tendency to form a $(\sqrt{3}\times\sqrt{3})$ordered structure in the plane. A cutoff distance of 10 Å was considered.

The potential energy $E^{I-I}$ of Equation 3b was included to emulate the electrostatic repulsion between Li atoms in different graphite layers. This potential energy follows a decreasing power law with distance, $r$, characterized by an $\alpha$ exponent and a term that attenuates the repulsive interactions at small distances, controlled by the parameter $\beta$. A cutoff distance of 26 Å, equivalent to 7 carbon planes, was used. $D_0$ and $r_b$ are two constant parameters.

The third term, $E^{A}$ in Equation 3c, is a constant parameter, which considers the interaction energy of Li atoms with the graphite substrate. In the present study, this term is not relevant, since all intercalation sites are a priori equivalent.

**Table I. Parameter values used in the simulations ($T$ = 296 K).**

| $\varepsilon$ | $r_m$[Å] | $D_0$ | $r_b$ | $\beta$ | $\alpha$ | $\gamma$ |
|---|---|---|---|---|---|---|
| $k_BT$ | 4.26 | $10k_BT$ | 1 | 1 | 2/3.15 | $-1.176k_BT$ |

Table I shows the values used for the present parameterization and Figure 2b shows the different potential terms in a schematic way.

***Model and computational methods.—***In order to analyze the Li intercalation process in a preexisting graphite substrate, a lattice-gas model is defined. Each intercalation site is at the center of the carbon hexagons (see Figure 1b), at a distance between planes – z axis - which is equal to half the distance between two adjacent graphite layers with AA stacking. This produces a triangular geometry lattice in each plane of $M = 12\times12\times24$ intercalation sites. The intercalation process is emulated using the Monte Carlo technique in the Grand Canonical assembly (GCMC).[27–29] In this system, graphite is considered in contact with an infinite Li reservoir at a temperature $T$ = 296 K and a chemical potential $\mu_{Li}$. The Metropolis algorithm was used to satisfy the detailed balance principle.[30] A Monte Carlo step was counted when each of the M sites has been evaluated to change their occupancy state. $1\times10^8$ MCGC steps were needed to guarantee the convergence of the simulation. An equal number of MCGC steps was used to obtain the averages of the variables to be measured. To explore the configuration space in an efficient way, the following computational procedure was implemented:

- *Step 1*. Given a configuration $\Omega$, a site $i$ is randomly chosen between the $M$ lattice sites.
- *Step 2*. A new configuration $\Omega^*$ is generated, by changing the occupation state of the site $i$.
- *Step 3*. The acceptance probability, $w_{\Omega\to\Omega^*}$, from the transition $\Omega$ to $\Omega^*$, is evaluated according to:

$$w_{\Omega\to\Omega^*} = \min\{1, \exp[-(\Delta U - \mu)/k_BT]\}$$

where $\Delta U = U(\Omega^*) - U(\Omega)$ is the potential energy difference between the configurations.

- *Step 4*. Steps 1 to 3 are repeated $M$ times.
- *Step 5*. Given a configuration $\Gamma$, a pair of planes $j$ and $k$ are randomly chosen between the 24 planes. If both planes are empty, two planes are chosen again until at least one of them is occupied.
- *Step 6*. A new configuration $\Gamma^*$ is generated by exchanging the occupation state of the planes $j$ and $k$.
- *Step 7*. The acceptance probability, $h_{\Gamma\to\Gamma^*}$, is evaluated according to:

$$h_{\Gamma\to\Gamma^*} = \min\{1, \exp[-\Delta U/k_BT]\}$$

where $\Delta U = U(\Gamma^*) - U(\Gamma)$ is the potential energy difference between the configurations.

- *Step 8*. Steps 5 to 7 are repeated 24 times.
- *Step 9*. Steps 1 to 8 are repeated $1\times10^7$ times.

The system Hamiltonian is:

$$H = \frac{1}{2}\left[\sum_{i}^{M}\sum_{j\neq i}^{M^{IP}} c_i c_j E_{ij}^{L-J} + \sum_{i}^{M}\sum_{j}^{M^{OP}} c_i c_j E_{ij}^{I-I}\right] + \sum_{i}^{M} c_i E_i^{A} \quad [4]$$

where $M$ = 3456 corresponds to the total number of intercalation sites. $M^{IP}$ is a subgroup of $M$ that includes only neighbor sites in the same plane of $i$. $M^{OP}$ is other subgroup of $M$, but contemplates sites in different planes from the site $i$. $c_k$ may take two possible values:

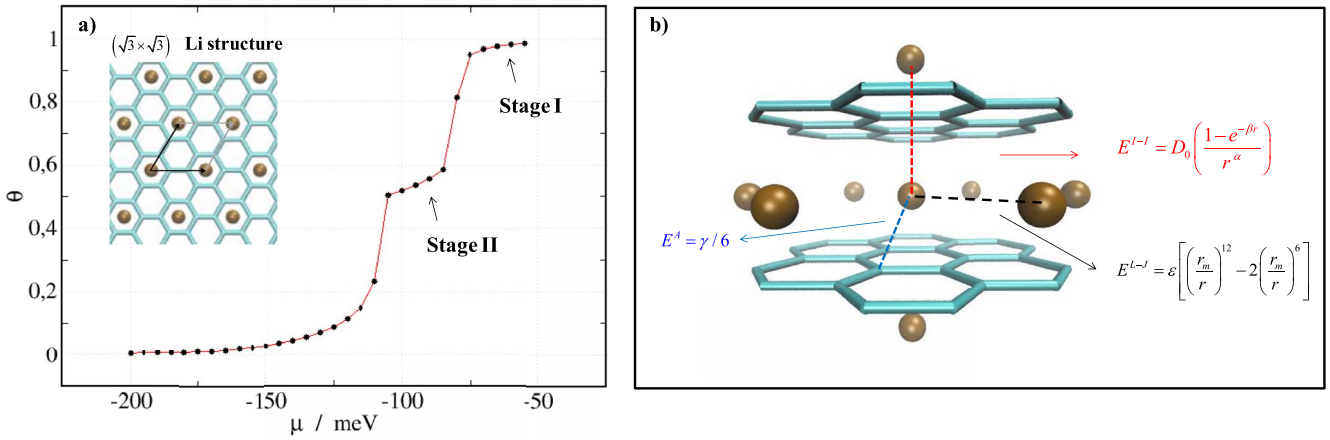


**Figure 2.** a) Isotherm for lithium intercalation in graphite, simulated in a Gran Canonical ensemble at 296 K, using the parameterization given in Table I with $\alpha = 3.15$. Inset show the 2D structure growth in Stage II and Stage I. b) Scheme of the potential contribution terms.

- $c_k = 0$ if the site $k$ is empty.
- $c_k = 1$if the site is occupied.

The intercalation isotherms, $\theta_{Li_XC_6}$ vs $\mu_{Li}$, were obtained as a simple average of each GCMC simulations,

$$\theta_{Li_XC_6}(\mu_{Li}, T) = \frac{3}{M}\left\langle \sum_i^M c_i \right\rangle = \frac{3\langle N\rangle}{M} \quad [5]$$

where $N$ is the number of Li atoms intercalated in the lattice-gas. The factor "3" is a normalization number, such that: $\theta_{Li_XC_6} = 1$, when stage I is formed.

The intercalation energy per atom, $U_{Li}$, was calculated as:

$$U_{Li} = \frac{1}{N}\left[\left\langle U^{Li_xC_6}\right\rangle - \left\langle U^{C_6}\right\rangle\right] \quad [6]$$

where $U^{Li_xC_6}$ y $U^{C_6}$ are the potential energy of lithium+graphite and graphite, respectively. In the present work $U^{C_6} = 0$.

The partial molar entropy was calculated from fluctuations as:[31]

$$\left(\frac{\partial S}{\partial x}\right)_{V,T} = \frac{1}{T}\left[\frac{\langle UN\rangle - \langle U\rangle\langle N\rangle}{\langle N^2\rangle - \langle N\rangle^2} - \mu\right] \quad [7]$$

Here $U$ is the total energy of the system, and $N$ the number of lithium ions intercalated in the lattice. $\mu$ is the chemical potential and $x$ correspond to the molar fraction. The symbol $\langle\rangle$ represents the average value of the property considered.

## Results

Figure 2 shows the intercalation isotherm, $\theta_{Li_XC_6}$, as a function of Lithium chemical potential, $\mu_{Li}$, using the parameters of Table I, with $\alpha = 3.15$, at 296 K. Three plateaus can be clearly identified, which corresponds to stages Id (gas-type), II (compact) and I (compact). As shown in the inset of Figure 2a, the system naturally adopts the $\left(\sqrt{3}\times\sqrt{3}\right)R30^{o}$ characteristic structure of the intercalation process of Li in graphite, for compact stages. All stages will be described in detail in the following sections. The complete intercalation process, from the beginning of the random deposition of gas Li atoms (stage Id) to the complete filling of stage I, takes place in a chemical potential range of $\Delta\mu_{Li} = (\mu^{I} - \mu^{Id}) \approx 150$ meV. This value agrees with experimental data.[12]

The $\alpha$ exponent, from Equation 3b, controls the electrostatic repulsion between Li atoms in distinct planes. It is, therefore, responsible for the $\Delta\mu_{Li}$ value, in such way that, when $\alpha$ decreases, the repulsion between Li atoms intensifies and $\Delta\mu_{Li}$ increases. Figures 2a and 3a show two intercalation isotherms for $\alpha = 3.15$ and $\alpha = 2$, respectively, using the same values for the other parameters. At first sight, it can be seen that at relatively low $\alpha$quantities, processes that were previously "hidden" in a small range of chemical potential start to be defined. We must clarify that, although the isotherm obtained with $\alpha = 2$ does not emulate the natural repulsion of the Li/graphite system between planes, its analysis will allow us to obtain

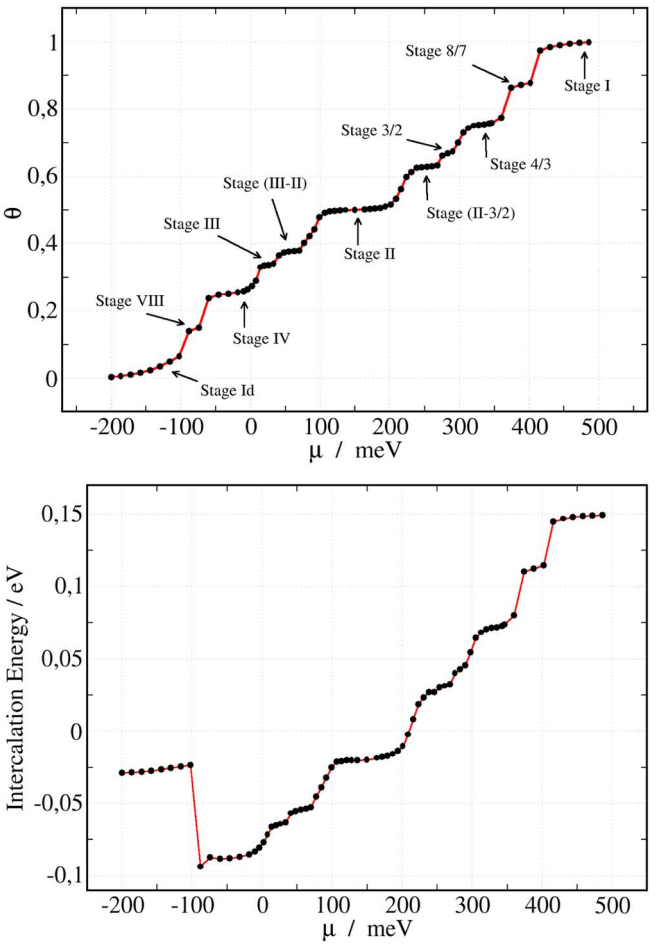


**Figure 3.** a) Isotherm for lithium intercalation in graphite, and b) intercalation energy as a function of chemical potential of Li, simulated in a Gran Canonical ensemble at 296 K. Using the parameterization given in Table I, with $\alpha = 2$.

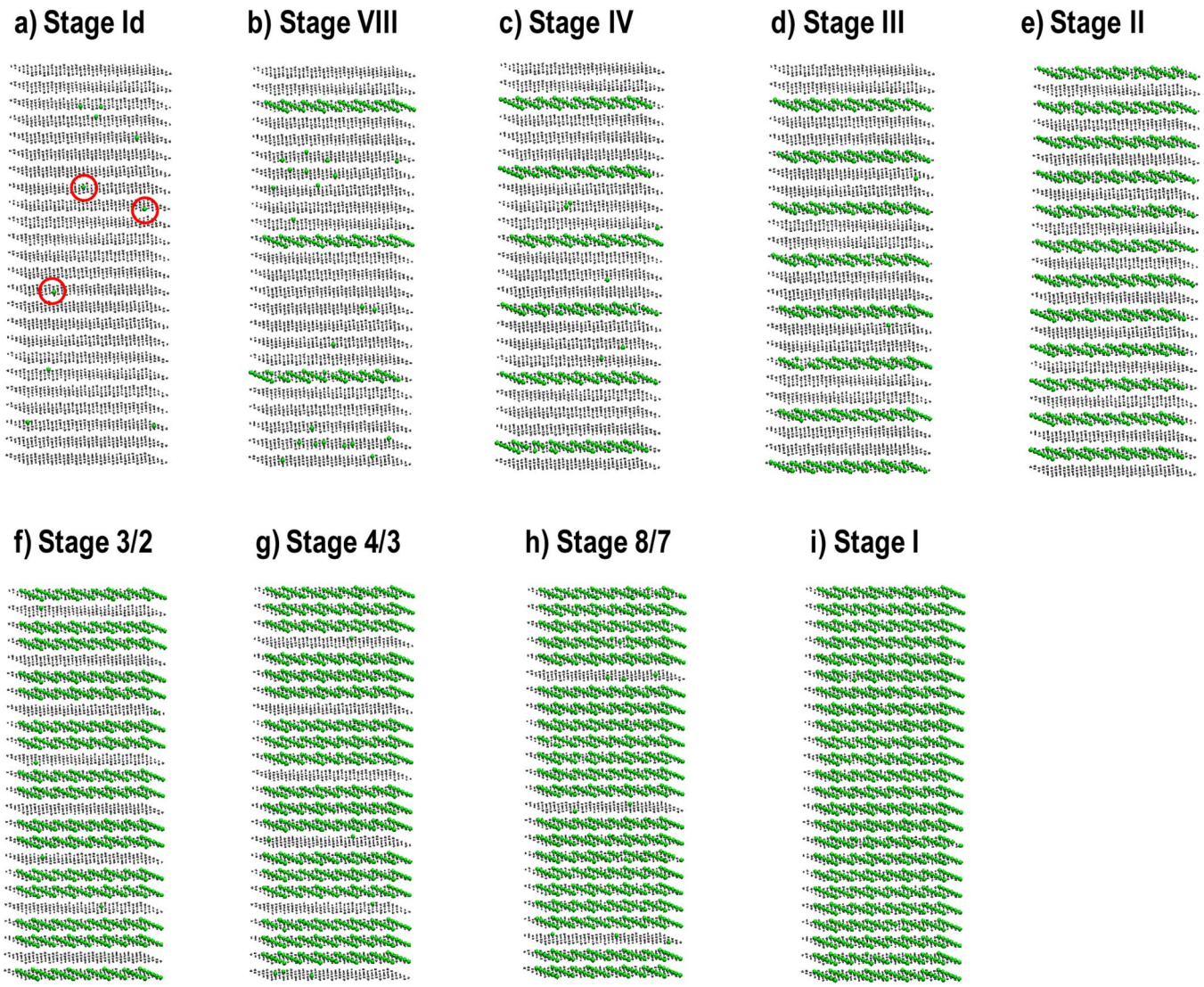


**Figure 4.** Snapshots from MC simulations, showing different structures associated with the isotherm plateaus in Figure 3a. The gray spheres correspond to empty intercalation sites and the gray ones to Li atoms. C atoms are not shown.

an important insight into the processes occurring during the intercalation process.

Several plateaus can be identified in Figure 3a, which are all related to different lithium-graphite stable structures. Each jump in the isotherm (from one plateau to another) is associated with transitions between these stages. Figure 3b shows the intercalation energies per particle, $U_{Li}$, defined previously in Eq. 6. On the other hand, Table II describes the stages names, the coverage values obtained from our simulations and the potential intercalation energies calculated for pure stages. Figures 4 and 5 shows representative images of the structures obtained in the different plateaus.

The entire intercalation process occurs along a range $\Delta\mu_{Li} = (\mu^{I} - \mu^{Id})$, a little higher than 700 meV. While only the parameter $\alpha$ has been modified in Eq. 3b, the energy inputs of the terms given in (3a) and (3c) were not altered, so both isotherms begin at the same point.

For a proper understanding of the insertion mechanism, a detailed analysis of all stages will now be done.

***First stage*** $(0 \rightarrow I_d)$**.—**At lithium coverages between $0 < \theta_{Li_XC_6} < 0.1$ a random distribution of Li atoms in bulk graphite takes place (stage $I_d$). A snapshot of this configuration is shown in Figure 4a, where some Li atoms have been marked with red circles. Experimental evidence of this stage has been previously reported in Literature.[32] It can be noted that $\theta_{Li_XC_6}$ grows as $\mu_{Li}$ moves to more positive values; the intercalation energy (Figure 3b) is negative, demonstrating the predominance of the energetic term Li-C (Eq. 3c) at this Li concentration. In addition, the intercalation energy presents a small positive slope, due to a small increase of the repulsive component from the out-of-plane interactions (Eq. 3b).

***Transition*** $(I_d \rightarrow VIII)$ **.—**The first jump until a plateau at $\theta_{Li_XC_6} \approx 0.125$, corresponds to the transition from the disordered state $I_d$ to a $(\sqrt{3} \times \sqrt{3})$ ordered structure, denominated here stage VIII. A representative image of this stage can be seen in Figure 4b. As the stage name alludes, the graphite sheets become occupied by Li ions every eight graphite planes. In concordance with Figure 4b, Figure 3b shows an abrupt change to more negative values in the intercalation energy at the chemical potential where the stage VIII is formed, which results from an increase in the attractive "in-plane" interactions, Eq. 3a. As lithium sheets are separated by seven empty intercalation planes, repulsive interactions are negligible.

***Transition*** $(VIII \rightarrow IV)$ **.—**At chemical potentials close to −65 meV, the transition from stage VIII to stage IV occurs. As expected,

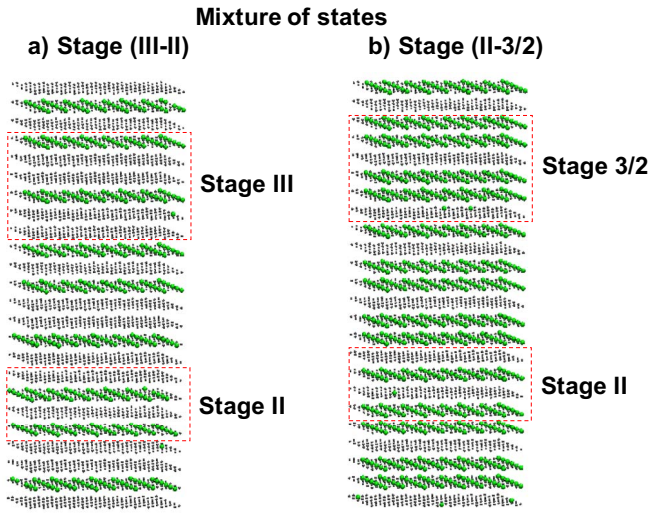


**Figure 5.** Snapshots showing stage mixtures. The colors of the spheres are the same as those detailed in Figure 4.

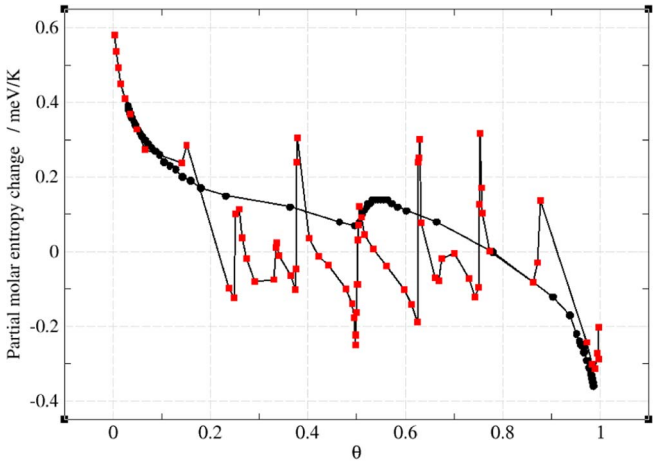


**Figure 6.** partial molar entropy change as a function of the amount of intercalated Li, using the parameterization given in Table I, with $\alpha = 2$ (red) and $\alpha = 3.15$ (black).

in stage IV the Li-occupied with the $(\sqrt{3} \times \sqrt{3})$ structure is repeated every 4 planes of graphite. As can be seen in Figure 4c, the lithium occupation is in this case, $\theta_{Li_XC_6}$, is 0.25.

***Transition*** $(IV \rightarrow III)$ **.—**At higher chemical potentials, close to $\mu_{Li} \approx 10$ meV a transition involving stage IV (Figure 4c) and stage III (Figure 4d) occurs. At the stage III plateau, $\theta_{Li_XC_6} \approx 0.333$. The intercalation energy is negative, but greater than the intercalation energy of stage IV, due to the increase in the contribution of the repulsive term, Eq 3b.

***Transition*** $(III \rightarrow II)$ **.—**A detailed examination reflects that this transition occurs by a mechanism involving a mixed stage between stages III and II. This "mixted" stable arrangement, stage (III-II), appears around $\mu_{Li} \approx 60$ meV. Figure 5a shows a snapshot extracted from the simulations, where the mixture of both phases can be observed. The transition $III \rightarrow II$implies that stage III is progressively "disordered" while stage II is "being ordered". The large number of possible configurations for the coexistence of these stages, generates a computational problem, making it difficult to explore the configuration space. This is the main reason why the planes exchange algorithm was implemented, as mentioned in section Model and computational methods.

***Transition*** $(II \rightarrow I)$**.—**Going back to the description of the intercalation isotherms, given in Figures 3a, we can identify three fractional stages (3/2, 4/3 and 8/7) and a mixed stage (II-3/2), in the interval $\mu_{Li} \approx 200$ meVto $\mu_{Li} \approx 500$ meV. Representative images of these stages are shown in Figures 4f–4h and Figure 5b, respectively. These partially unfilled stages exhibit a symmetry with respect to partially filled stages. In fact, they can be obtained by exchanging holes with particles in the stages previous to stage II, thus:

- Stage 3/2, is symmetric with stage III.
- Stage 4/3, is symmetric with stage IV.
- Stage 8/7, is symmetric with stage VIII.

Following the same analysis, the stage (II-3/2) is symmetrical with the stage (III-II).

***Partial molar entropy.—***Figure 6 shows the partial molar entropy, obtained according in Equation 7, as a function of the degree of intercalation, $\theta_{Li_XC_6}$, for the two models analyzed here: black dots for $\alpha = 3.15$ and red dots for $\alpha = 2$. As expected, the increase in the repulsive interaction forces, $(\alpha = 3.15 \rightarrow \alpha = 2.0)$ strongly affects the partial molar entropy of intercalation. As discussed in detail in References 33 and 34, the steps observed in the differential entropy indicate transitions between different intercalation phases. Its origin can be understood on the basis of configurational contributions, according to Yazami and Reynier's conjecture.[36] For $\alpha = 3.15$ curve, the differential entropy presents a step at $\theta_{Li_XC_6} : 0.5$, consistent with the transition from state II to I. On the other hand, several other steps appear for $\alpha = 2$, each of them associated to a plateau of the isotherm of Figure 3a. The increased repulsion between lithium ions in different graphite planes, causes that transitions become more abrupt, as was demonstrated by statistical mechanics models.[32]

It is remarkable that experimental differential entropies, such as those shown in Figure 4b in Reference 35, present small shoulders, before and after of $\theta_{Li_XC_6} : 0.5$, that give indication for the presence of new phases. Remarkably the experimental behavior is intermediate the curves shown in Figure 6.

***Stage (IV-II) and (IV-II)****.—Before the implementation of the algorithm descripted in section Model and computational methods, the system was simulated with the traditional Grand Canonical ensemble using the classical Metropolis algorithm, i.e., without steps 5 to 8, in the same conditions at the same temperature. The existence of mixed stages was found, mixtures of stages IV and II (stage IV-II) and its conjugated one, the stage (IV-II)*, but no signs of stage III. We show in Figure 7 two intercalation isotherms, $\theta_{Li_XC_6}$ vs $\mu_{Li}$, set up under the above conditions. There, we compare the results of the algorithm, with and without the steps 5 to 8, described in section Model and computational methods. We found that the plateaus at (25 meV; 0.38) and (275 meV; 0.66), in the black curve, disappear when the plane exchange algorithm is implemented, demonstrating that these plateaus

**Table II. Stage description, coverage degree, chemical potential at a coverage step to form the stage plateau and intercalation energy per particle for the pure stage.**

| Stage | $\theta_{Li_XC_6}$ | $\mu_{Li}$/meV | $U_{Li}$/meV atom$^{-1}$ |
|---|---|---|---|
| Id | <0.02 | −200 | |
| VIII | 0.125 | −90 | −114 |
| IV | 0.25 | −56 | −93 |
| III | 0.33 | 0 | −70 |
| II | 0.50 | 156 | −23 |
| 3/2 | 0.66 | 250 | 40 |
| 4/3 | 0.75 | 293 | 68 |
| 8/7 | 0.875 | 381 | 111 |
| I | 1.0 | 469 | 149 |

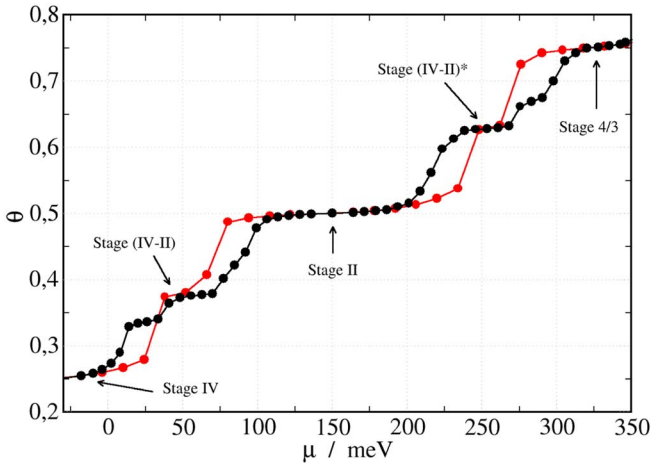


**Figure 7.** Isotherm for lithium intercalation in graphite simulated in a "traditional" (no steps 5 to 8) Gran Canonical ensemble using (black) exchange and (red) classical Metropolis scheme at 296 K.

correspond to metastable states. On the other hand, the thermodynamic stability of all state (there shown) change. In Figure 8 we presents the snapshot of mixed states (IV-II) and (IV-II)*.

From these findings, we thought it could be plausible to find a lower (pure) energy stage, since the system seemed to get "stuck" using this classical algorithm. So, the "plane exchange" step was implemented into the classical Metropolis algorithm to improve the relaxation method, and stage III, with a lower energy as compared with stage IV-II was found at practically the same chemical potential window. We found that while the pure state III has intercalation energy per particle of $-70$ meV atom$^{-1}$ (see Table II), the mixed state IV-II presents an intercalation energy per particle of $-55$ meV atom$^{-1}$. That result suggest that stage III is thermodynamically more stable than the mixed stage IV-II.

## Discussion

In the light of the observed mechanisms, we will try to analyze in this section what are the implications of the simulated stages for a laboratory experiment. To give an answer, we must return to the analysis given in Figure 2, where $\alpha = 3.15$ and the potential window is similar to the experimental window $\Delta\mu^{sim} \approx e_0 \Delta E^{\exp}$. The interval

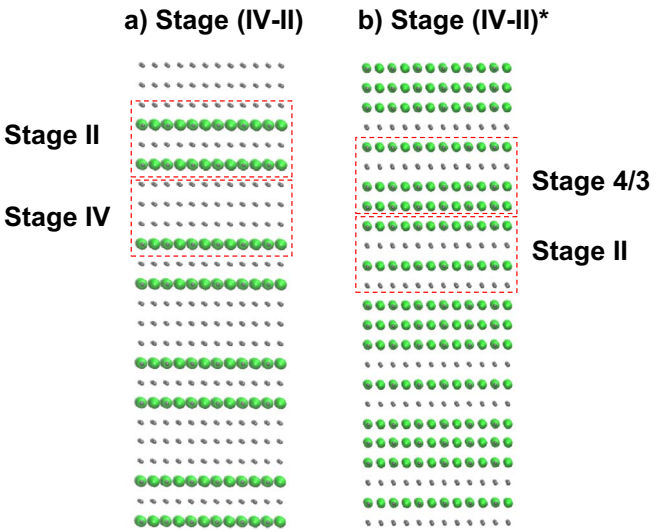


**Figure 8.** Snapshots showing mixed stages (IV-II) and (IV-II)*. The red rectangles show the different stage in coexistence.

$\Delta\mu^{Id\to II} = \mu^{II} - \mu^{Id}$ is slightly larger than 100 meV. In this interval, experimental evidence for states VIII, IV and III has been reported.

On the other hand, the transition $II \to I$ occurs in a potential window close to $\Delta\mu^{II\to I} \approx 25$ meV, comparable to the average thermal energy per atom: $k_B T \approx 25$ meV at 296 K. This makes it hard to identify the multiple stages in experiments at room temperature.

With respect to the transition between stages II to I, fractional stages have been reported, although their stoichiometry has not been identified yet.[35] From the analysis of entropy and crystal structure anomalies and impedance spectroscopy, Yazami and Reynier have fractional stages in the range of Li composition from 0.5 to 1.0.[36–38] Other authors have also found evidence for the existence of these stages by analyzing the effects of intercalation at low temperatures[39] or proposed their occurrence through DFT calculations.[19] On the other hand, the experimental visualization of the intermediate stages between stages I and II is very complex since, in addition to the contribution of the configurational energy (as presented here), there are also contributions due to excess energy that emerges as result of stress due to the deformation of graphite layers.[40]

It must also be mentioned that there is recent evidence[17] for a new intercalation mechanism, which involves the formation of stages IV-II and (IV-II)* instead of stages III and 3/2. We have shown that stage IV-II is not the most stable thermodynamic structure, as compared with stage III, but it may be occurring due to kinetic factors that frustrate the system, making it difficult to obtain the stage III arrangement.

In summary, the information presented here, added to that suggested by different experiments mentioned above, allows us to propose that a possible mechanism for the intercalation of lithium in graphite, in the transition, $II \to I$, can be decomposed into the transition

Stage II $\to$ Stage 3/2 $\to$ Stage 4/3 $\to$ Stage 8/7 $\to$ Stage I

or

Stage II $\to$ Stage (IV $-$ II)* $\to$ Stage 4/3 $\to$ Stage 8/7 $\to$ Stage I

these decomposition are consistent with other graphite intercalation compounds pathways,[11,41] suggesting the existence of a general intercalation mechanism.

## Conclusions

We have used a modification of an interaction potential used to describe lithium insertion in graphite to show the possible occurrence of several intermediate structures between the currently proposed stage I and stage II structures. We propose the following two sequences as possible:

Stage VIII $\to$ Stage IV $\to$ Stage III $\to$ Stage II $\to$ Stage 3/2 $\to$ Stage 4/3 $\to$ Stage 8/7 $\to$ Stage I

and

Stage VIII $\to$ Stage IV $\to$ Stage IV $-$ II $\to$ Stage II $\to$ Stage (IV $-$ II)* $\to$ Stage 4/3 $\to$ Stage 8/7 $\to$ Stages I

The last one involves the existence of a new stage, recently proposed,[17] the stage IV-II. One or the other will appear depending on kinetic control.

All these stages involve a $(\sqrt{3} \times \sqrt{3})$ 2D-structure. Hence, the simulation provide understanding to the processes involved in a real Li-graphite anode. It is very likely that, although these stages exist, they remain "hidden" in experimental measurements since there are factors that destabilize their structures. These other physical effects must be considered in future modeling.

## Acknowledgments

The authors acknowledge financial support from Universidad Nacional de Santiago del Estero, under project CONICET PIP 0547/14, CONICET PIP 11220110100992, SECyT Universidad Nacional de Córdoba, Program BID (PICT 2012–2324, PICT 2015-1605), and PME: 2006-01581 of Argentina. The simulations were carried out on a HUAUKE parallel cluster located at Instituto de Bionanotecnología del NOA, Universidad Nacional de Santiago del Estero, Santiago del Estero, Argentina.

## ORCID

O. A. Oviedo https://orcid.org/0000-0003-0738-9760

## References


1. L. Ji, Z. Lin, M. Alcoutlabi, and X. Zhang, *Energy Environ. Sci.*, **4**, 2682 (2011).
2. S. Goriparti, E. Miele, F. De Angelis, E. Di Fabrizio, R. ProiettiZaccaria, and C. Capiglia, *J. Power Sourc.*, **257**, 421 (2014).
3. M. Srivastava, J. Singh, T. Kuila, R. K. Layek, N. H. Kim, and J. H. Lee, *Nanoscale*, **7**, 4820 (2015).
4. N-S Choi, J-G. Han, S-Y. Ha, I. Park, and C-K Back, *RSC Adv*. **5**, 2732 (2015).
5. T-F. Yi, S-Y. Yang, and Y. Xie, *J. Mater. Chem. A*, **3**, 5750 (2015).
6. R. Palacin, *J. Am. Chem. Soc.*, **137**, 3140 (2015).
7. P. B. Balbuena and Y. Wang, *Lithium-Ion Batteries: Solid-electrolyte interphase.*, Imperial College Press, London, England (2004).
8. M. D. Levi and D. Aurbach, *J. Electroanal. Chem.*, **421**, 79 (1997).
9. M. D. Levi, E. A. Levi, and D. Aurbach, *J. Electroanal. Chem.*, **421**, 89 (1997).
10. T. Ohzuku, Y. Iwakoshi, and K. Sawa, *J. Electrochem. Soc.*, **140**, 2490 (1993).
11. Y. Reynier, R. Yazami, and B. Fultz, *J. of Power Sources*, **119**, 850 (2003).
12. E. M. Perassi and E. P. M. Leiva, *Electrochem. Comm.*, **65**, 48 (2016).
13. C. D. Fuerst, J. E. Fische, J. D. Axe, J. B. Hastings, and D. B. Mc Whan, *Phy. Rev. Lett.*, **50**, 357 (1983).
14. D. P. DiVincenzo, C. D. Fuerst, and J. E. Fische, *Phys. Rev. B*, **29**, 1115 (1984).
15. Y. Imai and A. Watanabe, *J. of Alloys and Compounds*, **439**, 258 (2007).
16. K. Persson, Y. Hinuma, Y. S. Meng, A. Van der Ven, and G. Ceder, *Phys. Rev. B*, **82**, 125416 (2010).
17. D. Allart, M. Montaru, and H. Gualous, *Journal of The Electrochemical Society*, **165**(2), A380 (2018).
18. V. Pande and V. Viswanathan, arXiv preprint arXiv:1607.05658 (2016) - arxiv.org.
19. S. Thinius, M. M. Islam, P. Heitjans, and T. Bredow, *J. Phys. Chem. C*, **118**, 2273 (2014).
20. C. B. Robledo, M. Otero, G. Luque, O. Cámara, D. Barraco, M. I. Rojas, and E. P. M. Leiva, *Electrochim. Acta*, **140**, 232 (2014).
21. M. Raju, P. Ganesh, P. R. C. Kent, and A. C. T. van Duin, *J. Chem. Theory Comput.*, **11**, 2156 (2015).
22. P. A. Derosa and P. B. Balbuena, *J. of The Electrochem. Soc.*, **146**(10), 3630 (1999).
23. E. M. Gavilán Arriazu, B. A. López de Mishima, O. A. Oviedo, E. P. M. Leiva, and O. A. Pinto, *Phys. Chem. Chem. Phys.*, **19**, 23138 (2017).
24. M. P. Mercer, S. Finnigan, D. Kramer, D. Richards, and H. E. Hoster, *Electrochim. Acta*, **241**, 141 (2017).
25. S. Poovathingal, T. E. Schwartzentruber, S. G. Srinivasan, and A. C. T. van Duin, *J. Phys. Chem. A*, **117**, 2692 (2013).
26. J. E. Lennard-Jones, *Cohesion, Proc. Phys. Soc.*, **43**(5), 461 (1931).
27. M. E. J. Newman and G. T. Barkema, *Monte Carlo Method in statistical physics*, Clarenton –Press Oxford, (1999).
28. H. B. Callen, "Thermodynamics and an introduction to thermostatistics", John Wiley & Sons, (1985).
29. D. Nicholson and N. G. Parsonage, "Computer Simulation and the Statistical Mechanics of Adsorption", Academic Press, London, (1982).
30. N. Metropolis, A. W. Rosenbluth, M. N. Rosenbluth, A. H. Tellery, and E. Teller, *J. Chem. Phys.*, **21**, 1087 (1953).
31. M. P. Mercera, S. Finnigana, D. Kramer, D. Richards, and H. E. Hoster, *Electrochim. Acta*, **241**, 141 (2017).
32. Y. Guo, R. B. Smith, Z. Yu, D. K. Efetov, J. Wang, P. Kim, M. Z. Bazant, and L. E. Brus., *J. Phys. Chem. Lett.*, **7**, 2151 (2016).
33. E. P. M. Leiva, E. Perassi, and D. Barraco, *J. Electrochem. Soc.*, **164**, A6154 (2017).
34. M. Otero, A. Sigal, E. M. Perassi, D. Barraco, and E. P. M. Leiva, *Electrochim. Acta*, **245**, 569 (2017).
35. F. Levy, *Intercalated layered materials*, first edition (1979).
36. R. Yazami and Y. Reynier, *J. of Power Sources*, **153**, 312 (2006).
37. Y. F. Reynier, R. Yazami, and B. Fultz, *J. of The Electrochem. Soc.*, **151**(3), A422 (2004).
38. R. Yazami, A. Martinent, and Y. F. Reynier, *Ionics*, **8**, 344 (2002).
39. A. Senyshyn, M. J. Mühlbauer, O. Dolotko, and H. Ehrenber, *J. of Power Sources*, **282**, 235 (2015).
40. E. V. Vakarin and J. P. Badiali, *J. Phys. Chem. B*, **106**(32), 7722 (2002).
41. L. Beneš, K. Melánová, V. Zima, J. Kalousová, and J. Votinský, *J. Inclusion Phenom. Mol. Recognit. Chem.*, **31**, 275 (1998).